Applied Physics Letters

Interfacial wicking dynamics and its impact on critical heat flux of boiling heat transfer

Cite as: Appl. Phys. Lett. **105**, 191601 (2014); https://doi.org/10.1063/1.4901569
Submitted: 14 July 2014 . Accepted: 30 October 2014 . Published Online: 10 November 2014

Beom Seok Kim, Hwanseong Lee, Sangwoo Shin, Geehong Choi, and Hyung Hee Cho

AIP Publishing

Interfacial wicking dynamics and its impact on critical heat flux of boiling heat transfer

Beom Seok Kim,[1] Hwanseong Lee,[1] Sangwoo Shin,[2] Geehong Choi,[1] and Hyung Hee Cho[1,a)]

[1]*Department of Mechanical Engineering, Yonsei University, 50 Yonsei-ro, Seodaemun-gu, Seoul 120-749, Korea*

[2]*Department of Mechanical and Aerospace Engineering, Princeton University, Princeton, New Jersey 08544, USA*

(Received 14 July 2014; accepted 30 October 2014; published online 10 November 2014)

Morphologically driven dynamic wickability is essential for determining the hydrodynamic status of solid-liquid interface. We demonstrate that the dynamic wicking can play an integral role in supplying and propagating liquid through the interface, and govern the critical heat flux (CHF) against surface dry-out during boiling heat transfer. For the quantitative control of wicking, we manipulate the characteristic lengths of hexagonally arranged nanopillars within sub-micron range through nanosphere lithography combined with top-down metal-assisted chemical etching. Strong hemi-wicking over the manipulated interface (i.e., wicking coefficients) of 1.28 $mm/s^{0.5}$ leads to 164% improvement of CHF compared to no wicking. As a theoretical guideline, our wickability-CHF model can make a perfect agreement with improved CHF, which cannot be predicted by the classic models pertaining to just wettability and roughness effects, independently. © *2014 AIP Publishing LLC*. [http://dx.doi.org/10.1063/1.4901569]

Nucleative boiling is definitely dependent on the interfacial hydrodynamics between phase-changing of fluids and counteracting re-wetting of the interface.[1] Two principal factors, which are surface morphology regarding roughness, and apparent wettability, have been the physical grounds to manipulate interfacial characteristics for favorable boiling performance. Advanced techniques, such as fabrication of nano/micro hierarchical structures,[2–4] and functionalization of interfaces allowed the synthesis of finer structures for limitless manipulation of interfaces, and secured the advantages of rough morphology and by-productive wetting characteristics for activating nucleation, areal pin-fin effects, and favorable surface re-wetting.[5–8]

Despite the promise of these approaches, the interfacial physics governing the thermo-hydraulic criteria on critical heat flux (CHF), which is the maximum heat dissipation capacity, remains poorly understood. When vigorous nucleation and its coalescence break the hydrodynamic stability, CHF will occur causing the burnout of the interface. Classical models are based on hydraulic instability and thermodynamic equilibrium states, and showed good coincidence with experimental results regarding macroscopic interfacial physics.[9–11] However, the classical models independently based on the apparent roughness and static wettability effects have fallen short of explaining unprecedented increases in CHF via nano-inspired interfaces. When nano- or nano-micro hierarchical structures realized extremely rough and superhydrophilic surfaces, the models had limitations to decrease an enormous discrepancy between the improved CHF and the predictions.[12,13]

The aim of this study is to suggest a reasonable approach to explain interfacial physics for predicting CHF, from the point of view of microscopic near-field mechanisms on hydrodynamic surface re-wetting. Particularly, we discuss how wickability driven by morphological aspects can be principal for determining the hydrodynamic refreshing capability over solid-liquid interfaces.[14–16] To control the wicking performance, arranged nanopillar structures were synthesized by top-down Si etching[5,17] with nanosphere lithography. Specifications and images of the structures are presented in Table I and Fig. 1, respectively. Detailed procedures for material preparations can be found in the supplementary information.[18]

The thermodynamic stability of a liquid droplet on a solid surface can be given by Young's equation as shown in Fig. 2(a), and it defines the physical characteristics of static contact angle (CA).[19] The hydrodynamic behavior of liquid should be governed by morphological characteristics regarding the surface roughness and porosity as well as the intrinsic characteristics such as interfacial free energies. Hydrophilicity is enhanced by roughening surface morphology based on Wenzel's model.[20] Especially, strong hydrophilicity can be realized when a geometrical prerequisite meets a criterion for the occurrence of hemi-wicking.[14,16] As described in Fig. 2(b), hemi-wicking is closely related to morphological factors. According to the Wenzel's model for

TABLE I. Geometrical variables and determinants for hemi-wicking of Eq. (1) on Si substrates with the manipulated nanopillars, and the resulting apparent CAs, θ.

	Geometric variables			Determinants for wicking			CAs
Case	d (nm)	p (nm)	h (nm)	r	φ	θ_c(°)	θ (°)
Case1	500	610	2000	10.75	0.61	87.8	10.5 ± 2.51
Case2	360	610	2000	8.02	0.32	84.9	9.56 ± 1.52
Case3	280	610	2000	6.46	0.19	82.7	6.97 ± 1.83

a)Author to whom correspondence should be addressed. Electronic mail: hhcho@yonsei.ac.kr. Tel.: +82 2 2123 2828. Fax: +82 2 312 2159.

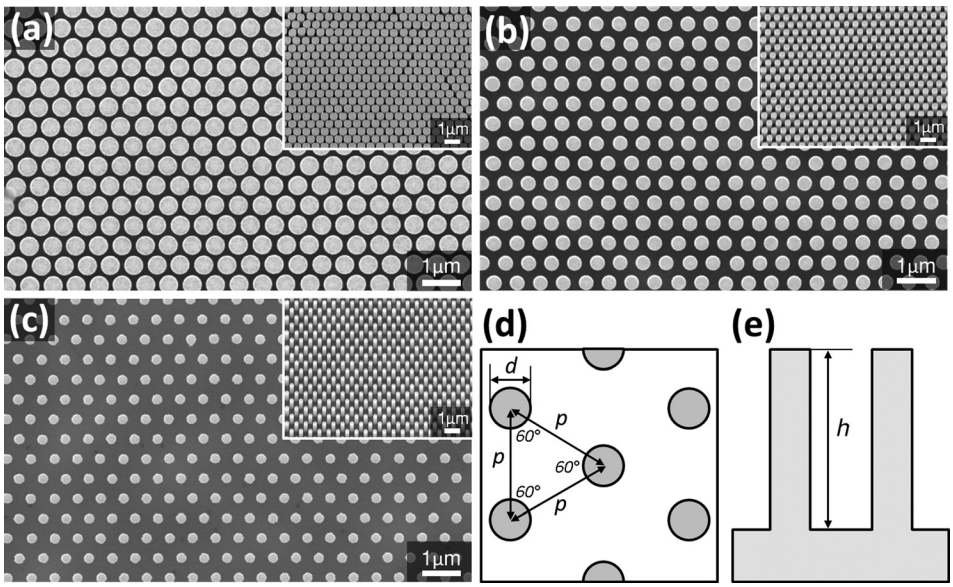

FIG. 1. SEM images of nanopillars with the same 610-nm pitch and 2-μm height: (a) case 1 diameter is 500 nm; (b) case 2 is 360 nm; (c) case 3 is 280 nm; (d) and (e) schematics describing nanopillars.

the equilibrium of interfacial forces, the criterion for hemi-wicking can be expressed as a function of geometric variables[14,16]

$$\theta^* < \theta_c \ (\cos\theta_c = (1-\varphi)/(r-\varphi)), \tag{1}$$

where θ^*, θ_c, r, and φ represent the equilibrium CA on an ideal plain surface, critical CA demanded as the prerequisite, roughness factor defined as the ratio of the actual to projected surface area, and solid fraction of the solid-liquid interface contacting the liquid droplet, respectively. Considering the average diameter d, pitch p, and height h of the hexagonally arranged pillars described in Figs. 1(d) and 1(e), we define the determinants of $r \equiv 1 + (\pi dh/p^2 \sin 60)$ and $\varphi \equiv (\pi d^2/4p^2 \sin 60)$ as the function of variables. The Si substrate has an equilibrium CA of 42.6°, and we can readily increase the hydrophilicity by extremely roughening the morphology, leading to hemi-wicking. These deliver the conditions for wicking characteristics for Eq. (1) with critical CAs higher than 80° for all of the manipulated nanopillars (Table I). Since the geometric prerequisite satisfies the criterion of hemi-wicking, we can see from Figs. 2(c) and S2(a)–S2(c) that water can be permeated immediately on the interface having the nanopillars (multimedia view).[18]

Because the wicking is laminar flow, the liquid supply to the wicking front can be linearly related to hydraulic

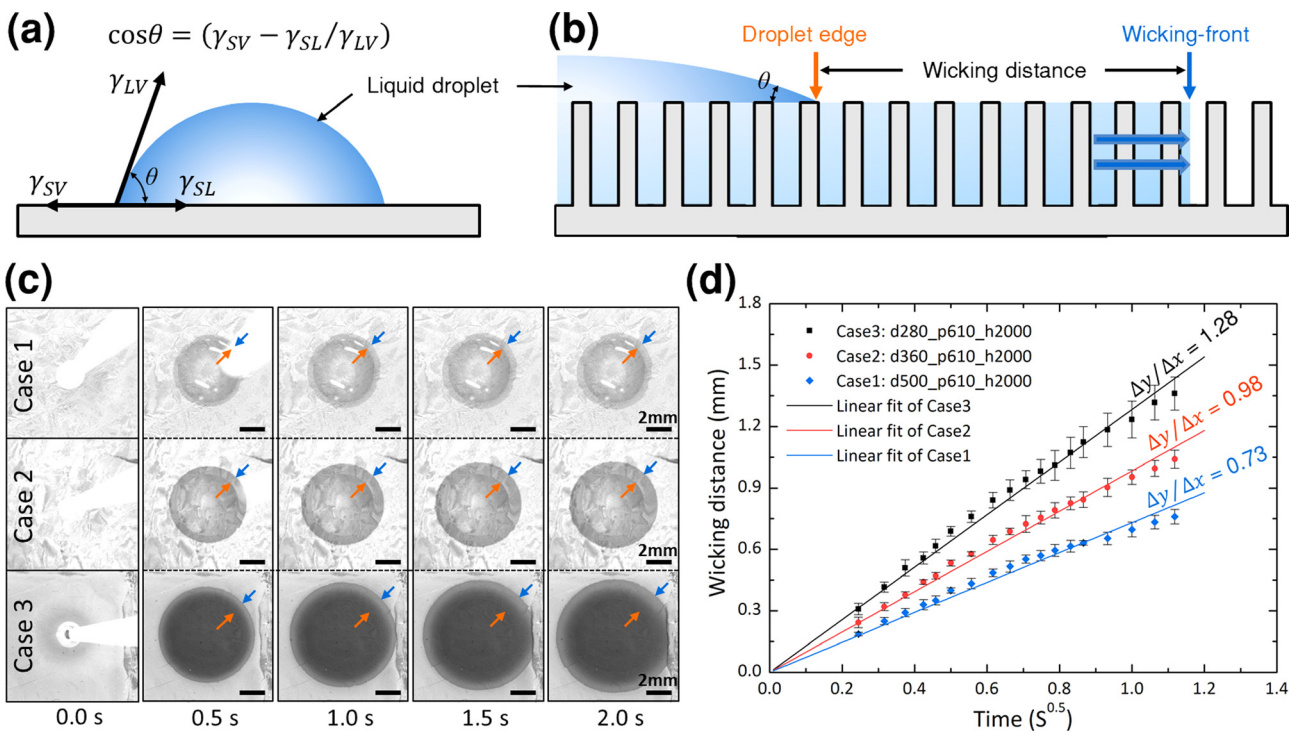

FIG. 2. Wetting and hemi-wicking: (a) and (b) schematic describing the thermodynamic stability of a droplet on a solid and hemi-wicking on a roughened surface; (c) wicking by a water droplet on the nanopillars. Movies are attached in the supplementary material;[18] (d) wicking propagation plots. The wicking coefficient (W) is defined by the average slope of wicking distance versus the square root of time.

resistance for a fully developed flow. When we assume that the wicking through interfacial structures is a Poiseuille flow on a plain surface, wickability is dependent on the fluidic resistance and the capillary pressure based on the Washburn model.[21,22] Then, the wicking distance, x, can be expressed as a function of time and characteristic lengths of wicking passages as follows:[23]

$$x = \left(\frac{2}{3\beta}\cdot\frac{\cos\theta^* - \cos\theta_c}{\cos\theta_c}\cdot\frac{\gamma h}{\mu}\cdot t\right)^{0.5} = W\cdot t^{0.5}, \quad (2)$$

where β, γ, μ, t, and W are the empirically determined constant, surface tension of the liquid, viscosity of the liquid, time, and wicking coefficient, respectively. Here, β is a kind of shape factor regarding dimensions and shape of a capillary-inducing structures.[24–27] If the volume of liquid droplet is sufficient and the wicking passage has a rectangular cross-section for straight forward propagation, the wicking coefficient can be characterized by controlling the spacing between nanopillars. Figures 2(c) and 2(d) show that the nanopillars lead to interfacial hemi-wicking, and consequent wicking coefficients of 0.73, 0.98, and 1.28 mm/s$^{0.5}$, respectively. Satisfying the prerequisite for hemi-wicking, expanding space between nanopillars can reinforce the wickability by decreasing hydraulic resistance. This is in a good agreement with previous demonstrations that reducing resistance against liquid propagation is essential to enhance wicking performance.[22,24] Lowering the hydraulic resistance also results in the reinforcement of static hydrophilicity with apparent CAs of 10.5°, 9.56°, and 6.97° from three cases, respectively.

The effect of the wicking manipulation on CHF can be verified through the evaluation of boiling curves as presented in Fig. 3 showing the relationship between an applied heat flux and a corresponding wall superheat.[18] Considering this critical point of CHF, we confirm from Fig. 3 that CHF gradually increases as we reinforce hemi-wicking performance. CHF is a key parameter for a reliable heat dissipating boiling system. It is a physical phenomenon involving the hydrodynamic characteristics of phase-change and fluid momentum[28–30] as well as surface characteristics.[5,6,12] Considering the hydraulic stability between evaporative nucleation and accessibility of coolant,[28,29] and interfacial characteristics

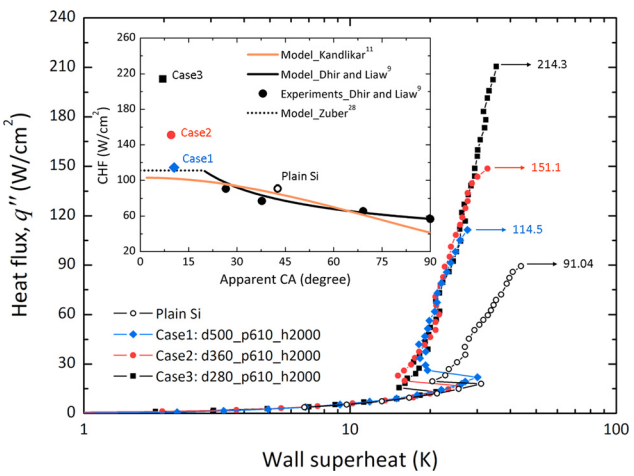

FIG. 3. Boiling curves from the manipulated surfaces. Inset presents the comparison between experimental and predicted CHF values.

such as the apparent static wetting,[9,11] numerous approaches have been modified to how thermo-hydrodynamics and its instability affect CHF, and to accurately predict CHF. While far-filed mechanisms are explaining hydrodynamic instabilities between up-flowing vapors and counteracting down-flowing liquids, near-field mechanisms focus on interfacial effects over a boiling surface excluded in far-field physics.[5] One accepted approach by Kandlikar describes the behavior of a bubble on a vapor-liquid interface, and considers the interfacial hydrodynamics to define critical condition of CHF.[11] In particular, Dhir and Liaw also presented that CA is a principal determinant of the hydrodynamics regarding the size of nucleating bubbles.[9] They established a model based on theoretical approximations of heat transfer rate through the conduction of liquid layer and its evaporation. On the models, interfacial hydrodynamics reflecting inherent characteristics of a boiling surface were indirectly regarded by considering contact angle, and have been effective to guide experimental CHF results. However, we can find that macroscopic approaches on hydrodynamic behavior by itself is insufficient to explain the remarkable increase in CHF obtained especially by nano-inspired interfaces.[12] As we also presented in the inset of Fig. 3, they show considerable discrepancies compared to the theoretical predictions, which considered apparent CA as a principal determinant. The discrepancy is getting larger in strong hydrophilic regime. These results prompt us to ask whether these disparities arise from a factor that was excluded from the prediction, without regard to the characteristics of the hydrodynamic interface such as static wetting of apparent CAs. However, the wetting is not an independent factor, but is coupled to the topography of surfaces.[14,16,25] Intuitively, we therefore suspect the influential factor will be the roughness. The observed CHF improvements in Fig. 3 cannot be explained independently by the roughness factor, either. CHF clearly increased, although r decreased from case 1 to case 3. This apparent contradiction was also discussed in recent studies indicating that the roughness cannot independently dominate in predicting CHF, but it should be manipulated to obtain favorable surface porosity and capillary pumping effects.[4,7,13,31]

Since roughness and wettability are correlated, especially in terms of wickability, the re-wetting by hemi-wicking accounts for the disparity regarding liquid propagation and supply into an interfacial layer. CHF occurs when a surface cannot guarantee accessibility of liquid-phase coolant against the dry-out of a surface, by the excessive depletion rate of the liquid over the supply of a coolant toward the surface.[32,33] The refreshing capacity and rate of coolant within the interface can be modeled based on the morphologically driven wicking, and the total amount of heat dissipation can then be quantitatively analyzed. The interface with arranged nanostructures is porous and thus has the volumetric capacity to be filled by wicking. Herein, the amount of liquid supply on a confined area can be formulated by the void fraction $(1-\varphi)$ and the height of the interfacial layer substituted by the height of interfacial structures (h). First, the refreshing rate of a liquid can be expressed pertaining to the dynamic characteristics of the wicking based on wicking coefficients (W), which is an integral driving force for supplying liquid. Assuming that hemi-wicking occurs with a uniform velocity profile along a

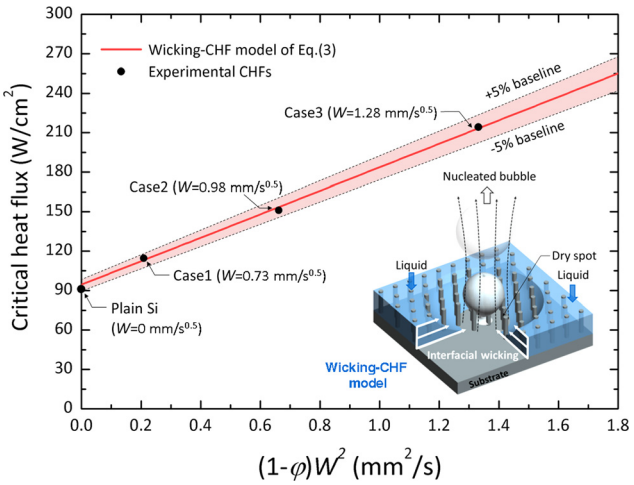

FIG. 4. Theoretical approximation of CHFs. The red solid line is an approximation by the wicking-CHF model of Eq. (3). The dashed lines indicate ±5% disparity from the model.

vertical direction within a thin interface, the total amount of heat absorption by the refreshing liquid, i.e., heat dissipation capacity by the evaporation, can be expressed as $(l_{lg}\rho_l)\cdot((1-\varphi)h)\cdot W^2$. The hydrodynamic stability is guaranteed on a confined area with the Rayleigh–Taylor interfacial wavelength of λ_{RT} describing the critical length for initiating instability between up-flowing vapor and down-flowing liquid.[10,11] The analytical expression for the enhancement of CHF can then be expressed by augmenting the heat dissipation capacity from a plain surface as follows:

$$q''_{wick-CHF} = Bl_{lg}\rho_l(1-\varphi)W^2/\lambda_{RT}^2 + q''_{Kandlikar,\,CHF}|_{plain}, \quad (3)$$

where $q''_{wick-CHF}$, l_{lg}, and ρ_l are the critical heat flux value by the wicking model, latent heat of fluid, and density of liquid-phase fluid, respectively. Here, B corresponds to a compensating factor for the wicking capacity regarding the height of the interface as $C_1\cdot h$, and is empirically fitted by 0.102 for 2 μm height layer by hexagonally arranged nanopillars. From Fig. 4, we confirm that the wickability can establish well-matched CHF criteria as a linear function. The y-axis intercept of the linear fit (94.4 W/cm^2) also corresponds well with the empirical CHF of 91.0 W/cm^2 on a plain surface (3.60% difference), which does not involve wicking behavior at all. This term refers to the reference condition without any wicking, and it can be reflected by Kandlikar's model as inserted in the right-hand side of Eq. (3).

Strong wicking can enhance boiling performance by guaranteeing hydrodynamic stability against surface dry-out. Wickability can thus be essential for a model to account for the hydrodynamic criteria on CHF regarding interfacial liquid propagation and refreshment. In this study, we discussed that the interfacial hydrodynamics can be physically approximated by the wicking induced by morphological-aspects of the surface, i.e., the wicking coefficient was an integral factor for quantizing re-wetting of the interface. The amount of refreshing water within a boiling interface could be predicted by the wickability, and it could be related to the criteria of CHF considering the instability of the hydrodynamic behavior of the multiphase flow. We suggested that the wickability-CHF model to demonstrate the dynamic wicking factor is linearly related to CHF, and strong wickability can lead to outstanding CHF values which cannot be predicted by the classic models pertaining to just wettability or roughness effects, independently. We expect it to be a starting point to explain the physics of CHF with respect to the hydrodynamic concept of wickability, which combines the effects of surface roughness and wettability over manipulated interfaces.

This work was supported by a National Research Foundation of Korea (NRF) grant funded by the Korea government (MEST) (No. 2011-0017673) and the Human Resources Development program (No. 20144030200560) of the Korea Institute of Energy Technology Evaluation and Planning (KETEP) Grant funded by the Korea government Ministry of Trade, Industry and Energy.

[1]V. K. Dhir, Annu. Rev. Fluid Mech. **30**, 365 (1998).
[2]B. S. Kim, S. Shin, S. J. Shin, K. M. Kim, and H. H. Cho, Nanoscale Res. Lett. **6**, 333 (2011).
[3]S. Shin, B. S. Kim, G. Choi, H. Lee, and H. H. Cho, Appl. Phys. Lett. **101**, 251909 (2012).
[4]K. Chu, Y. S. Joung, R. Enright, C. R. Buie, and E. N. Wang, Appl. Phys. Lett. **102**, 151602 (2013).
[5]M. C. Lu, R. K. Chen, V. Srinivasan, V. Carey, and A. Majumdar, Int. J. Heat Mass Transfer **54**, 5359 (2011).
[6]C. Li, Z. Wang, P. I. Wang, Y. Peles, N. Koratkar, and G. P. Peterson, Small **4**, 1084 (2008).
[7]K. Chu, R. Enright, and E. N. Wang, Appl. Phys. Lett. **100**, 241603 (2012).
[8]B. S. Kim, S. Shin, D. Lee, G. Choi, H. Lee, K. M. Kim, and H. H. Cho, Int. J. Heat Mass Transfer **70**, 23 (2014).
[9]V. K. Dhir and S. P. Liaw, J. Heat Transfer **111**, 739 (1989).
[10]S. G. Liter and M. Kaviany, Int. J. Heat Mass Transfer **44**, 4287 (2001).
[11]S. G. Kandlikar, J. Heat Transfer **123**, 1071 (2001).
[12]R. Chen, M. C. Lu, V. Srinivasan, Z. Wang, H. H. Cho, and A. Majumdar, Nano Lett. **9**, 548 (2009).
[13]H. Hanley, C. Coyle, J. Buongiorno, T. McKrell, L. Hu, M. Rubner, and R. Cohen, Appl. Phys. Lett. **103**, 024102 (2013).
[14]J. Bico, U. Thiele, and D. Quéré, Colloids Surf. A **206**, 41 (2002).
[15]F. C. Cebeci, Z. Z. Wu, L. Zhai, R. E. Cohen, and M. F. Rubner, Langmuir **22**, 2856 (2006).
[16]B. S. Kim, S. Shin, S. J. Shin, K. M. Kim, and H. H. Cho, Langmuir **27**, 10148 (2011).
[17]S. Kim and D. Khang, Small **10**, 3761 (2014).
[18]See supplementary material at http://dx.doi.org/10.1063/1.4901569 for the synthesis of nanopillars, experimental details on characterization, boiling experimental facilities, data reduction, uncertainty analysis, and supplementary movies on wicking propagation.
[19]Z. Yoshimitsu, A. Nakajima, T. Watanabe, and K. Hashimoto, Langmuir **18**, 5818 (2002).
[20]R. N. Wenzel, Ind. Eng. Chem. **28**, 988 (1936).
[21]E. W. Washburn, Phys. Rev. **17**, 273 (1921).
[22]N. R. Tas, J. Haneveld, H. V. Jansen, M. Elwenspoek, and A. van den Berg, Appl. Phys. Lett. **85**, 3274 (2004).
[23]J. Bico, C. Tordeux, and D. Quéré, Europhys. Lett. **55**, 214 (2001).
[24]C. Ishino, M. Reyssat, E. Reyssat, K. Okumura, and D. Quéré, Europhys. Lett. **79**, 56005 (2007).
[25]D. Quéré, Annu. Rev. Mater. Res. **38**, 71 (2008).
[26]C. Zhang and C. H. Hidrovo, *ASME 2009 Second International Conference on Micro/Nanoscale Heat and Mass Transfer* (American Society of Mechanical Engineers, 2009), Vol. 3, p. 423.
[27]T. T. Mai, C. Q. Lai, H. Zheng, K. Balasubramanian, K. C. Leong, P. S. Lee, C. Lee, and W. K. Choi, Langmuir **28**, 11465 (2012).
[28]N. Y. Zuber, AEC Report AECU-4439 (1959).
[29]A. E. Bergles and W. M. Rosenow, J. Heat Transfer **86**, 365 (1964).
[30]C. C. Hsu and P. H. Chen, Int. J. Heat Mass Transfer **55**, 3713 (2012).
[31]H. S. Ahn, H. J. Jo, S. H. Kang, and M. H. Kim, Appl. Phys. Lett. **98**, 071908 (2011).
[32]M. G. Cooper and J. M. D. Merry, Int. J. Heat Mass Transfer **16**, 1811 (1973).
[33]C. Gerardi, J. Buongiorno, L. Hu, and T. McKrell, Int. J. Heat Mass Transfer **53**, 4185 (2010).